

ARFlow: Human Action-Reaction Flow Matching with Physical Guidance

Wentao Jiang¹ Jingya Wang^{1*} Kaiyang Ji¹ Baoxiong Jia² Siyuan Huang² Ye Shi^{1*}

¹ShanghaiTech University ²Beijing Institute for General Artificial Intelligence

{jiangwt2024, wangjingya, jiky2024, shiye}@shanghaitech.edu.cn
{jiabaoxiong, syhuang}@bigai.ai

Abstract

Human action-reaction synthesis, a fundamental challenge in modeling causal human interactions, plays a critical role in applications ranging from virtual reality to social robotics. While diffusion-based models have demonstrated promising performance, they exhibit two key limitations for interaction synthesis: reliance on complex noise-to-reaction generators with intricate conditional mechanisms, and frequent physical violations in generated motions. To address these issues, we propose Action-Reaction Flow Matching (ARFlow), a novel framework that establishes direct action-to-reaction mappings, eliminating the need for complex conditional mechanisms. Our approach introduces a physical guidance mechanism specifically designed for Flow Matching (FM) that effectively prevents body penetration artifacts during sampling. Moreover, we discover the bias of traditional flow matching sampling algorithm and employ a reprojection method to revise the sampling direction of FM. To further enhance the reaction diversity, we incorporate randomness into the sampling process. Extensive experiments on NTU120, Chi3D and InterHuman datasets demonstrate that ARFlow not only outperforms existing methods in terms of Fréchet Inception Distance and motion diversity but also significantly reduces body collisions, as measured by our new Intersection Volume and Intersection Frequency metrics. Our project is available at <https://arflow2025.github.io/>.

1 Introduction

Human action-reaction synthesis [59, 72, 10] has emerged as a pivotal research direction in computer vision [70, 39, 58, 28, 60, 67]. This task aims to generate physically plausible human reactions responding to observed actions, with critical applications in virtual reality, human-robot interaction, and character animation. Unlike single-human motion generation [19, 62, 8], reactors must infer responses without observing future actor motions, creating unique modeling challenges.

While recent diffusion methods [62, 72] show promise in motion generation, they face two key limitations in the modeling of action-reaction interactions. First, existing approaches [62, 72] indirectly model responses using noise-to-reaction generators with intricate conditional mechanisms like treating action information as a condition to guide the generation process. This not only complicates the training process but also fails to directly capture the inherent causal relationship between actions and reactions. Second, frequent physical violations like body penetration between characters occur due to neglected physical constraints. While such issues are absent in single-human scenarios, they become critical in human interaction applications [26]. This poses a significant barrier

*Corresponding authors.

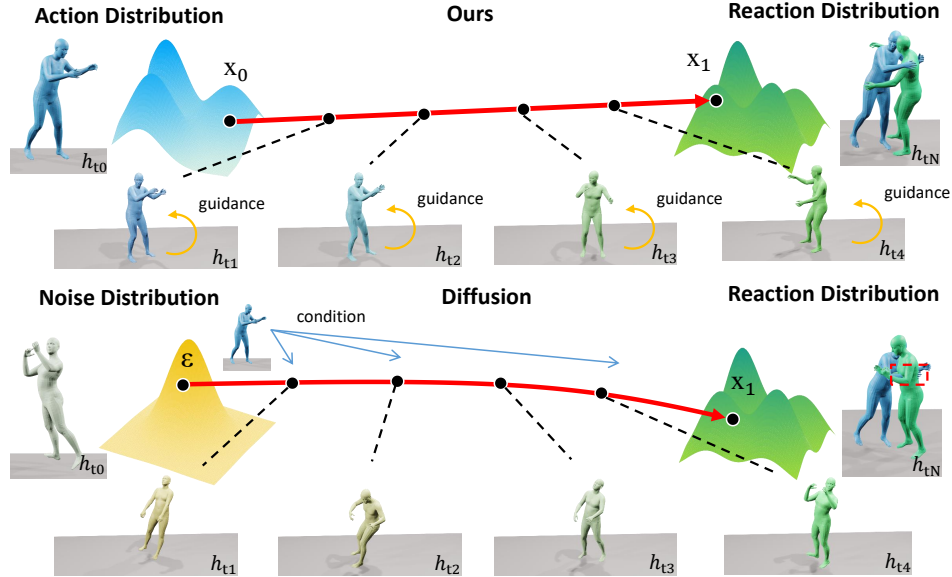


Figure 1: Our proposed Human Action-Reaction Flow (**ARFlow**). We directly establish a mapping between the action and reaction distribution and our sampling process is further guided by our physical constraint guidance. The change of colors represents the variation of the h -frame reaction with sampling timestep t_n .

to real-world applications such as virtual reality and human-robot interaction, where even minor physical inaccuracies are intolerable [53, 26].

To address these challenges, we propose Action-Reaction Flow Matching (ARFlow), a novel framework that fundamentally resolves these limitations. Unlike diffusion models constrained by noise-data mappings, flow matching [40, 44, 1, 48] naturally models paired distributions through linear interpolation between endpoints (See Fig. 1), making it inherently suitable for action-reaction synthesis. ARFlow establishes direct pathways between action and reaction distributions, enabling simpler training and faster inference compared to diffusion-based methods. Instead of traditional vector field prediction (v-prediction) in standard flow matching [40, 27], ARFlow directly outputs clean body poses (x_1 -prediction) in human motion generation. To eliminate unrealistic body collisions between characters, we further develop a specialized sampling algorithm that performs physical constraint guidance at x_1 to avoid inaccurate gradients, and projects it back onto a revised Flow Matching path through interpolation. This innovation maintains physical plausibility through gradient guidance without compromising motion quality. Additionally, we introduce two new physics-aware evaluation metrics: Intersection Volume (IV) and Intersection Frequency (IF). Our main contributions are threefold:

- We propose ARFlow, the first Flow Matching architecture that creates direct pathways between human action and reaction distributions, eliminating the need for complex conditional mechanisms prevalent in diffusion approaches.
- We integrate physical constraints and employ a reprojection method to revise the sampling direction of FM, surpassing vanilla guidance methods. This successfully prevents body collisions between characters while preserving natural movement. To further enhance the reaction diversity, we introduce randomness into the sampling process.
- We introduce two new evaluation metrics (IV, IF) for interaction quality assessment. Experiments demonstrate state-of-the-art performance in Fréchet Inception Distance (FID), MultiModality (Multimod.), IV and IF on NTU120 and Chi3D datasets.

2 Related Work

2.1 Human Motion Generation

Human motion synthesis aims to generate diverse and realistic human-like motion conditioned on different guidances, including text [79, 21, 33, 14], music [83, 37], speech [22, 4], sparse signals

[15, 61], action labels [19, 50, 62, 6, 8], or unconditioned [51, 62, 74]. Recently, many diffusion-based motion generation models have been proposed [78, 62, 14, 8, 69, 63] and demonstrate better quality compared to alternative models such as VAE [34, 19, 50, 6], flow-based models [54, 3] or GANs [74, 70]. Alternatively, motion can be regarded as a new form of language and embedded into the language model framework [77, 29].

Meanwhile, the exploration of guiding the sampling process of diffusion models [12, 75] has been a key area in motion diffusion models, PhysDiff [31] proposes a physics-guided motion diffusion model, which incorporates physical constraints in a physics simulator into the diffusion process. GMD [31] presents methods to enable spatial guidance without retraining the model for a new task. DNO [31] proposes a motion editing and control approach by optimizing the diffusion latent noise of an existing pre-trained model.

2.2 Human Action-Reaction Synthesis

Different from human-human interaction [70, 39, 58, 28, 60, 67], human action-reaction synthesis is causal and asymmetric [72, 42, 71]. To address this task, researchers have leveraged large language models [57, 59, 30], VAE-based methods [10, 45, 46]. However, these methods cannot capture fine-grained representations and ensure diversity, and diffusion-based methods [38, 60] are limited to the “offline” and “constrained” setting of human reaction generation, failing to generate instant and intention agnostic reactions. More recently, ReGenNet [72] introduce a diffusion-based transformer decoder framework and treat action sequence as conditional signal for online reaction generation. However, it often produce physically-implausible inter-penetrations between the actor and reactor since they disregard physical constraints in the generative process. Our method addresses this problem by ARFlow sampling with physical constraint guidance.

2.3 Flow Matching

Flow Matching [40, 44, 1, 48, 47, 17] has emerged as an efficient alternative to diffusion models, offering linear generation trajectories through ODE solvers. This paradigm enables simplified training and accelerated inference [16, 41], with successful applications spanning images [40, 16], audio [36], video [5], and point clouds [68]. In motion generation, MotionFlow [27] demonstrates comparable performance to diffusion models with faster sampling. Notably, Flow Matching inherently models transitions between arbitrary distributions through transport maps, making it particularly suitable for paired data modeling. Despite these advantages, its potential for action-reaction synthesis remains unexplored. Our work bridges this gap by establishing direct action-to-reaction mappings without complex conditional mechanisms.

3 Method

In the setting of human action-reaction synthesis, our primary goal is to generate the reaction $\mathbf{x}_1 = \{x_1^i\}_{i=1}^H$ conditioned on an arbitrary action $\mathbf{x}_0 = \{x_0^i\}_{i=1}^H$ of length H . The condition \mathbf{c} can be action \mathbf{x}_0 , or it can be a signal such as an action label, text, audio to instruct the interaction, which is optional for intention-agnostic scenarios. We utilize SMPL-X [49] human model to represent the human motion sequence as [72] to improve the modeling of human-human interactions. Thus, the reaction can be represented as $x_1^i = [\theta_i^{x_1}, \mathbf{q}_i^{x_1}, \gamma_i^{x_1}]$ where $\theta_i^{x_1} \in \mathbb{R}^{3K}$, $\mathbf{q}_i^{x_1} \in \mathbb{R}^3$, $\gamma_i^{x_1} \in \mathbb{R}^3$ are the pose parameters, the global orientation, and the root translation of the person, respectively. Total number K of body joints, including the jaw, eyeballs, and fingers, is 54. The main pipeline of our ARFlow model is provided in Fig. 2. In this section, we first introduce the Human Action-Reaction Flow Matching in Sec. 3.1. Then, we present our training-free physical constraint guidance method to address the issue of physically implausible human-human inter-penetrations in Sec. 3.2.

3.1 Human Action-Reaction Flow Matching

Flow Matching Overview. Given a set of samples from an unknown data distribution $q(\mathbf{x})$, the goal of flow matching is to learn a *flow* that transforms a prior distribution $p_0(\mathbf{x})$ towards a target data distribution $p_1(\mathbf{x}) \approx q(\mathbf{x})$ along the probability path $p_t(\mathbf{x})$. The time-dependent flow $\phi_t(\mathbf{x})$ is defined by a vector field $\mathbf{v}(\mathbf{x}, t) : \mathbb{R}^d \times [0, 1] \rightarrow \mathbb{R}^d$ which establishes the flow through a neural ODE:

$$\frac{d}{dt}\phi_t(\mathbf{x}) = \mathbf{v}(\phi_t(\mathbf{x}), t), \quad \phi_0(\mathbf{x}) = \mathbf{x}. \quad (1)$$

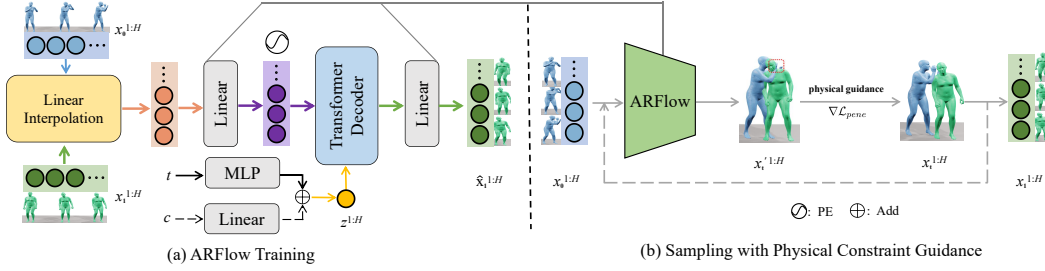


Figure 2: **Pipeline of ARFlow.** (a) For a sampled timestep t , we linearly interpolate a coupled action-reaction pair as Eq. 4 to produce the intermediate state $x_t^{1:H}$, which is then turns into a d -dimensional latent feature through a linear layer. We use Transformer Decoder Units to directly predict clean reaction motions. (b) After training the networks in (a), our ARFlow uses them for sampling, which is further guided by the gradient of \mathcal{L}_{pene} to generate physically plausible reactions.

Given a predefined probability path $p_t(\mathbf{x})$ and a corresponding vector field $\mathbf{u}_t(\mathbf{x})$, one can regress the vector field $\mathbf{u}_t(\mathbf{x})$ with a neural network $\mathbf{v}_\theta(\mathbf{x}_t, t)$ parameterized by θ , and the Flow Matching (FM) objective is as follows:

$$\min_{\theta} \mathbb{E}_{t, p_t(\mathbf{x})} \|\mathbf{v}_\theta(\mathbf{x}_t, t) - \mathbf{u}_t(\mathbf{x})\|^2. \quad (2)$$

By defining the conditional probability path as a linear interpolation between p_0 and p_1 , the intermediate process becomes: $\mathbf{x}_t = t\mathbf{x}_1 + [1 - (1 - \sigma_{\min})t]\mathbf{x}_0$, where $\sigma_{\min} > 0$ is a small amount of noise. Both training and sampling are simplified by fitting a linear trajectory in contrast to diffusion paths. When extra condition signals \mathbf{c} are required, they can be directly incorporated into the vector field estimator $\mathbf{v}_\theta(\mathbf{x}_t, t)$ as $\mathbf{v}(\mathbf{x}_t, t, \mathbf{c})$. Therefore, the training objective is as follows:

$$\min_{\theta} \mathbb{E}_{t, p(\mathbf{x}_0), q(\mathbf{x}_1)} \left\| \mathbf{v}_\theta(\mathbf{x}_t, t, \mathbf{c}) - \left(\mathbf{x}_1 - (1 - \sigma_{\min})\mathbf{x}_0 \right) \right\|^2. \quad (3)$$

Action-Reaction Flow Matching. Different from previous diffusion-based methods[72, 62, 38, 15] that rely on cumbersome conditional mechanisms, we adopt Flow Matching to directly construct a mapping from action distribution to reaction distribution (See Fig. 1). Specially, we build a generative model f parametrized by θ to synthesize the reaction $\mathbf{x}_1 = f_\theta(\mathbf{x}_0, \mathbf{c})$, given action \mathbf{x}_0 , instead of $\mathbf{x}_1 = f_\theta(\mathbf{z}, \mathbf{c})$ in diffusion, given a sampled Gaussian noise vector \mathbf{z} . Given the reaction \mathbf{x}_1 sampled from the reaction distribution and the coupled action \mathbf{x}_0 from the action distribution, the intermediate process can be written as

$$\mathbf{x}_t = t\mathbf{x}_1 + [1 - (1 - \sigma_{\min})t]\mathbf{x}_0, \quad (4)$$

where t is the timestep, $\sigma_{\min} > 0$ is a small amount of noise. In our setting, the generative process is conditionally formulated as $p(\mathbf{x}_{t_{n+1}} | \mathbf{x}_{t_n}, \mathbf{c})$. We use a neural network G to directly predict the clean body poses, *i.e.*, $\hat{\mathbf{x}}_1 = G_\theta(\mathbf{x}_t, t, \mathbf{c})$, instead of predicting vector fields in previous works [27, 40]. This strategy is both straightforward and effective, since many geometric losses directly act on the predicted $\hat{\mathbf{x}}_1$. We compared and analyzed the results of predicting vector fields (\mathbf{v} -prediction) and clean body poses (\mathbf{x}_1 -prediction) in Sec. 4.4. Note that \mathbf{x}_1 in flow matching usually corresponds to \mathbf{x}_0 in previous literature on diffusion models. Depending on the specific application, G can be implemented by Transformers [65] or MLP networks. The training objective of our flow model is as follows:

$$\mathcal{L}_{\text{fm}} = \mathbb{E}_{\mathbf{x}_1 \sim q(\mathbf{x}_1), \mathbf{x}_0 \sim p(\mathbf{x}_0), t \sim [0, 1]} [\|\mathbf{x}_1 - G_\theta(\mathbf{x}_t, t, \mathbf{c})\|_2^2]. \quad (5)$$

Following [72], we employ explicit interaction losses to evaluate the relative distances of body pose $\theta(\mathbf{x}_1, \mathbf{x}_0)$, orientation $q(\mathbf{x}_1, \mathbf{x}_0)$ and translation $\gamma(\mathbf{x}_1, \mathbf{x}_0)$ between the actor and reactor. We use a forward kinematic function to transforms the rotation pose into joint positions for calculating $\theta(\mathbf{x}_1, \mathbf{x}_0)$, and converts the rotation poses to rotation matrices for calculating $q(\mathbf{x}_1, \mathbf{x}_0)$. The interaction loss is defined as

$$\begin{aligned} \mathcal{L}_{\text{inter}} = & \frac{1}{H} \left(\|\theta(\mathbf{x}_1, \mathbf{x}_0) - \theta(\hat{\mathbf{x}}_1, \mathbf{x}_0)\|_2^2 \right. \\ & \left. + \|q(\mathbf{x}_1, \mathbf{x}_0) - q(\hat{\mathbf{x}}_1, \mathbf{x}_0)\|_2^2 + \|\gamma(\mathbf{x}_1, \mathbf{x}_0) - \gamma(\hat{\mathbf{x}}_1, \mathbf{x}_0)\|_2^2 \right). \end{aligned} \quad (6)$$

Our overall training loss is $\mathcal{L}_{\text{all}} = \mathcal{L}_{\text{fm}} + \lambda_{\text{inter}} \cdot \mathcal{L}_{\text{inter}}$, and λ_{inter} is the loss weight.

Sampling based on \mathbf{x}_1 -prediction. Since our neural network outputs $\hat{\mathbf{x}}_1$, we require to construct an equivalent relationship between the neural network’s predictions of \mathbf{v} and \mathbf{x}_1 . The equivalent form of parameterization Eq. 23 derived from our appendix is as follows:

$$\mathbf{v}_\theta(\mathbf{x}_t, t, c) = \frac{\hat{\mathbf{x}}_1 - (1 - \sigma_{\min})\mathbf{x}_t}{1 - (1 - \sigma_{\min})t}, \quad (7)$$

Then, our sampling based on \mathbf{x}_1 -prediction can be achieved by first sampling \mathbf{x}_0 and then solving Eq. 1 employing an ODE solver [55, 35, 2] through our trained neural network $\hat{\mathbf{x}}_1 = G_\theta(\mathbf{x}_t, t, c)$. We use the Euler ODE solver and discretization process involves dividing the procedure into N steps, leading to the following formulation:

$$\mathbf{x}_{t_{n+1}} \leftarrow \mathbf{x}_{t_n} + (t_{n+1} - t_n) \mathbf{v}_\theta(\mathbf{x}_{t_n}, t_n, \mathbf{c}), \quad (8)$$

where the integer time step $t_1 = 0 < t_2 < \dots < t_N = 1$. By using equivalent form of parameterization Eq. 7, we finally obtain our flow matching sampling formulation based on \mathbf{x}_1 -prediction:

$$\mathbf{x}_{t_{n+1}} \leftarrow \frac{1 - (1 - \sigma_{\min})t_{n+1}}{1 - (1 - \sigma_{\min})t_n} \mathbf{x}_{t_n} + \frac{t_{n+1} - t_n}{1 - (1 - \sigma_{\min})t_n} \hat{\mathbf{x}}_1, \quad (9)$$

which is more suitable for human motion generation. Detailed derivation is provided in **Appendix A**.

3.2 ARFlow Sampling with Physical Constraint Guidance

There exist many physically implausible inter-penetrations between the actor and reactor in the generated results of current diffusion-based methods [72, 62, 15], owing to the sampling process that disregards physical constraints. To address the issue, we employ a penetration gradients $\nabla \mathcal{L}_{\text{pene}}$ to guide the sampling process. We follow [32, 38] to calculate the signed distance function (SDF) between the actor and the reactor as our penetration loss function:

$$\mathcal{L}_{\text{pene}}(\mathbf{x}) := \sum_{i,h} -\min\left(\text{SDF}(\psi_i^h(\mathbf{x})), \zeta\right), \quad (10)$$

where $\psi_i^h(\mathbf{x})$ represents the position of the i -th joint in the h -th frame of the generated reaction motion \mathbf{x} , the ζ defines the safe distance between the actor and the reactor, beyond which the gradient becomes zero, and SDF is the signed distance function for an actor in the h -th frame, which dynamically changes across frames.

Traditional diffusion guidance methods [12, 31, 63] first estimate $\hat{\mathbf{x}}_1$ from current state \mathbf{x}_{t_n} with a denoiser network $\epsilon_\theta(\mathbf{x}_{t_n}, t_n, \mathbf{c})$, and then calculate gradients of the loss function with respect to current state \mathbf{x}_{t_n} , so it inevitably requires differentiation of the neural network, resulting in inaccurate gradients $\nabla \mathcal{L}_{\text{pene}}$. To avoid this issue, we directly updates the gradient at $\hat{\mathbf{x}}_1$:

$$\hat{\mathbf{x}}'_1 \leftarrow \hat{\mathbf{x}}_1 - \lambda_{\text{pene}} \nabla_{\hat{\mathbf{x}}_1} \mathcal{L}_{\text{pene}}(\hat{\mathbf{x}}_1), \quad (11)$$

where $\hat{\mathbf{x}}_1$ is the clean body poses predicted by our neural network G_θ and λ_{pene} is the guidance strength. Then, we use the linear interpolation of Flow Matching to project back to the intermediate state of learned FM path.

Interpolation between action and reaction. Since we build flow matching between the action and reaction distribution, unlike the process of adding noise back in diffusion, our interpolation process depends on the initial point \mathbf{x}_0 , so we need to project towards the direction of the initial point. The Flow Matching sampling algorithm Eq. 9 is equivalent to the following formulation:

$$\hat{\mathbf{x}}_0 \leftarrow \hat{\mathbf{x}}_1 + \frac{\mathbf{x}_{t_n} - (1 + \sigma_{\min}t)\hat{\mathbf{x}}_1}{1 - (1 - \sigma_{\min})t_n}, \quad (12)$$

$$\mathbf{x}_{t_{n+1}} \leftarrow t_{n+1}\hat{\mathbf{x}}_1 + [1 - (1 - \sigma_{\min})t_{n+1}] \hat{\mathbf{x}}_0. \quad (13)$$

This sampling process essentially finds a $\hat{\mathbf{x}}_0$ along the opposite direction of the current velocity field for linear interpolation as Eq. 12 (black dotted lines in Fig. 3). Obviously, this predicted $\hat{\mathbf{x}}_0$ deviates from the initial point \mathbf{x}_0 (purple dotted lines in Fig. 3). In order to correct the projection direction of traditional Flow Matching, we use a weight factor w to weight $\hat{\mathbf{x}}_0$ and \mathbf{x}_0 :

$$\hat{\mathbf{x}}_0^* \leftarrow w\hat{\mathbf{x}}_0 + (1 - w)\mathbf{x}_0. \quad (14)$$

and use $\hat{\mathbf{x}}_0^*$ as our final endpoint for interpolation. The ARFlow sampling and traditional sampling algorithm for \mathbf{x}_1 -prediction with physical constraint guidance are shown in Algorithm 2 and 1 respectively. In practice, we use \mathbf{x}_1 -prediction for its better performance. Under iterative sampling and physical constraint guidance, our method can generate more realistic and physically-plausible reaction motions.

Stochastic sampling to enhance diversity of reactions. To further enhance the diversity of reactions generated by ARFlow, we incorporate randomness into the sampling process. The interpolation Eq. 13 can be written in the following equivalent form:

$$\mathbf{x}_{t_{n+1}} \leftarrow \hat{\mathbf{x}}_1 + (1 - t_{n+1})(\hat{\mathbf{x}}_0 - \hat{\mathbf{x}}_1) + \sigma_{\min} t_{n+1} \hat{\mathbf{x}}_0. \quad (15)$$

The interpolation process can be understood as a projection in the opposite direction of the current learned velocity field $\hat{\mathbf{x}}_1 - \hat{\mathbf{x}}_0$. Thus, we can weight the projection direction $\hat{\mathbf{x}}_0^* - \hat{\mathbf{x}}_1'$ and stochastic direction d_{random} to incorporate randomness:

$$d_{\text{mix}} \leftarrow \hat{\mathbf{x}}_0^* - \hat{\mathbf{x}}_1' + \beta[d_{\text{random}} - (\hat{\mathbf{x}}_0^* - \hat{\mathbf{x}}_1')], \quad (16)$$

$$\mathbf{x}_{t_{n+1}} \leftarrow \hat{\mathbf{x}}_1' + (1 - t_{n+1})d_{\text{mix}} + \sigma_{\min} t_{n+1} \hat{\mathbf{x}}_0^*, \quad (17)$$

where β is the factor to control the strength of randomness. Our guidance method is actually a refined fine-tuning, which may be not suitable for training. In addition, the loss during the training mainly measures the difference between generated results and ground truth, while our guidance during the inference phase can provide more flexible guidance based on the quality of the generated results.

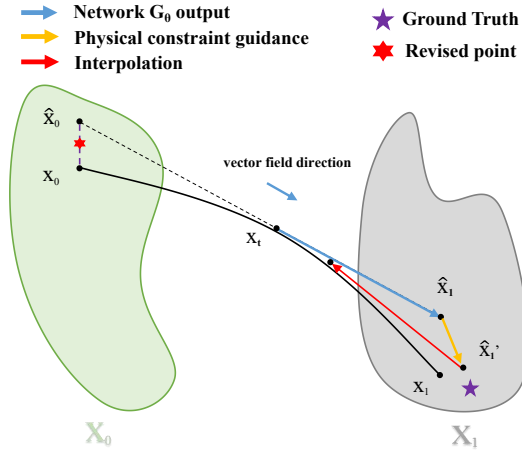


Figure 3: Illustration of our ARFlow sampling with physical constraint guidance.

	FID ↓	IF ↓	IV ↓
Real	0.09	21.96%	5.35
Offline			
MDM	22.04	15.45%	3.36
ReGenNet	6.19	19.14%	3.07
ARFlow	5.00	9.67%	1.94
MDM ^{vanilla}	20.42	13.29%	2.26
ReGenNet ^{vanilla}	7.69	17.85%	2.16
ARFlow ^{vanilla}	5.19	6.37%	0.31
ARFlow ^{improved}	5.05	3.73%	0.23
Online			
MDM	51.11	32.63%	17.97
ReGenNet	11.00	13.84%	3.50
ARFlow	7.89	8.39%	3.26
MDM ^{vanilla}	40.03	22.63%	10.35
ReGenNet ^{vanilla}	11.63	13.05%	2.71
ARFlow ^{vanilla}	8.61	3.29%	1.44
ARFlow ^{improved}	8.07	3.23%	0.53

Table 1: Human action-reaction synthesis with physical constraint guidance on NTU120-AS. **Bold** indicates the best result.

Metrics. To qualitatively measure the degree of penetration, we introduced two metrics:

1) **Intersection Volume (IV).** Penetrate in [76, 23] just measures ground penetration which is not suitable for measuring the degree of penetration between humans. Interpenetration in [46] can only be computed as rigid bodies in the physics simulation. Inspired by Solid Intersection Volume (IV) [81, 43], we measure human-human inter-penetration by voxelizing actor and reactor meshes and reporting the volume of voxels occupied by both. Intersection Volume (IV) is defined as

$$IV = \frac{1}{H \cdot N_{\text{total}}} \sum_{i=1}^{N_{\text{total}}} \sum_{h=1}^H V_{\text{pene}}^h, \quad (18)$$

where V_{pene}^h represents intersection volume of frame h and N_{total} denotes the total number of samples.

2) **Intersection Frequency (IF).** Inspired by Contact Frequency in [38, 57], we introduce IF to measure the frequency of inter-penetration, *i.e.*

$$IF = f_{\text{pene}} / F_{\text{total}}, \quad (19)$$

where f_{pene} represents the number of inter-penetration frames and F_{total} is the total number of frames.

Algorithm 1 Sampling algorithm with vanilla guidance of physical constraints.

```

1: Input:  $\mathcal{L}_{\text{pene}}$  the loss function ;  $G$  and  $\theta$  the clean
   body poses predictor with pretrained parameters
2: Parameters:  $N$  the number of sampling steps;
    $\lambda_{\text{pene}}$  the guidance strength
3: Sample  $\mathbf{x}_0$  from the action distribution
4: for  $n = 1, 2, \dots, N - 1$  do
5:    $\hat{\mathbf{x}}_1 \leftarrow G_\theta(\mathbf{x}_{t_n}, t_n, \mathbf{c})$ 
6:   # Flow Matching  $\mathbf{x}_1$ -prediction
   sampling (Eq. 9)
7:    $\mathbf{x}'_{t_{n+1}} \leftarrow \frac{1-t_{n+1}}{1-t_n} \mathbf{x}_{t_n} + \frac{t_{n+1}-t_n}{1-t_n} \hat{\mathbf{x}}_1$ 
8:   # Physical constraint guidance
9:    $\mathbf{x}_{t_{n+1}} \leftarrow \mathbf{x}'_{t_{n+1}} - \lambda_{\text{pene}} \nabla_{\hat{\mathbf{x}}_1} \mathcal{L}_{\text{pene}}(\hat{\mathbf{x}}_1)$ 
10: end for
11: Return: The reaction motion  $\mathbf{x}_1 = \mathbf{x}_{t_N}$ 

```

Algorithm 2 Sampling algorithm with improved guidance of physical constraints.

```

1: Input:  $\mathcal{L}_{\text{pene}}$  the loss function ;  $G$  and  $\theta$  the clean
   body poses predictor with pretrained parameters
2: Parameters:  $N$  the number of sampling steps;
    $\lambda_{\text{pene}}$  the guidance strength;  $w$  weight factor
3: Sample  $\mathbf{x}_0$  from the action distribution
4: for  $n = 1, 2, \dots, N - 1$  do
5:    $\hat{\mathbf{x}}_1 \leftarrow G_\theta(\mathbf{x}_{t_n}, t_n, \mathbf{c})$ 
6:    $\hat{\mathbf{x}}_0 \leftarrow \hat{\mathbf{x}}_1 + \frac{\mathbf{x}_{t_n} - (1 + \sigma_{\min} t) \hat{\mathbf{x}}_1}{1 - (1 - \sigma_{\min}) t_n}$  # (Eq. 12)
7:   # Physical constraint guidance at  $\hat{\mathbf{x}}_1$  (Eq. 11)
8:    $\hat{\mathbf{x}}'_1 \leftarrow \hat{\mathbf{x}}_1 - \lambda_{\text{pene}} \nabla_{\hat{\mathbf{x}}_1} \mathcal{L}_{\text{pene}}(\hat{\mathbf{x}}_1)$ 
9:   # Direction correction
10:   $\hat{\mathbf{x}}_0^* \leftarrow w \hat{\mathbf{x}}_0 + (1 - w) \mathbf{x}_0$ 
11:  # Interpolation (Eq. 13)
12:   $\mathbf{x}_{t_{n+1}} \leftarrow t_{n+1} \hat{\mathbf{x}}'_1 + [1 - (1 - \sigma_{\min}) t_{n+1}] \hat{\mathbf{x}}_0^*$ 
13: end for
14: Return: The reaction motion  $\mathbf{x}_1 = \mathbf{x}_{t_N}$ 

```

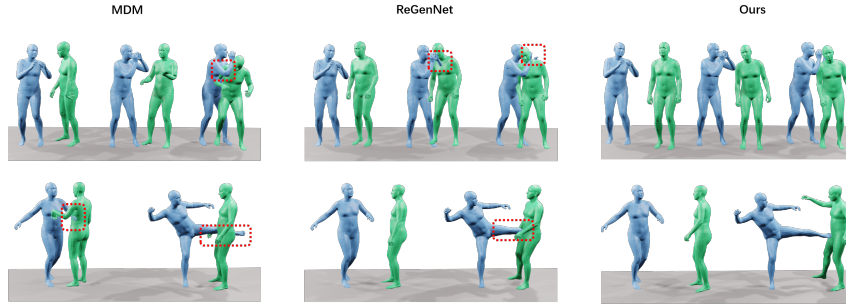


Figure 4: **Qualitative comparisons** of human action-reaction synthesis results. **Blue** for actors and **Green** for reactors.

4 Experiments

Our experiment setting of human action-reaction synthesis is **online** and **unconstrained** as in [72] for its significant potential for practical applications. **Online** represents real-time reaction generation where future motions of the actor are not visible to the reactor, and the opposite is **offline** to relax the synchronicity. **Unconstrained** means that the intention of the actor is invisible to the reactor. To demonstrate the universality of our flow matching and physical guidance methods, we also conducted offline setting experiments.

4.1 Experiment setup

Evaluation Metrics. 1) We adopt the following metrics to quantitatively evaluate results: Frechet Inception Distance (FID), Action Recognition Accuracy (Acc.), Diversity (Div.) and Multi-modality (Multimod.). For all these metrics widely used in previous human motion generation [19, 50, 62, 72], we use the action recognition model [73] to extract motion features for calculating these metrics as in [72]. We generate 1,000 reaction samples by sampling actor motions from test sets and evaluate each method 20 times using different random seeds to calculate the average with the 95% confidence interval as prior works [19, 50, 62, 72]. 2) **Intersection Volume (IV)** measures human-human inter-penetration by voxelizing actor and reactor meshes and reporting the volume of voxels occupied by both. 3) **Intersection Frequency (IF)** measures the frequency of inter-penetration. More details about these metrics are provided in the supplementary.

Datasets. We evaluate our model on NTU120-AS, Chi3D-AS and InterHuman-AS datasets with SMPL-X [49] body models and actor-reactor annotations as in [50]. They contain 8118, 373 and 6022 human interaction sequences, respectively. “AS” [72] represents that they are an extended version of the original dataset [18, 42, 64, 39], which adds annotations to distinguish actor-reactor order of each interaction sequence and SMPL-X body models for more detailed representations. We adopt the 6D rotation representation [82] in all our experiments.

Method	FID↓	Acc.↑	Div.→	Multimod.→
Real	0.09±0.00	0.867±0.0002	13.06±0.09	25.03±0.23
cVAE [34]	70.10±3.42	0.724±0.0002	11.14±0.04	18.40±0.26
AGRoL [15]	44.94±2.46	0.680±0.0001	12.51±0.09	19.73±0.17
MDM [62]	54.54±3.94	0.704±0.0003	11.98±0.07	19.45±0.20
MDM-GRU [62]	24.25±1.39	0.720±0.0002	13.43±0.09	22.24±0.29
ReGenNet [72]	<u>11.00±0.74</u>	0.749±0.0002	13.80±0.16	<u>22.90±0.14</u>
ARFlow	7.89±0.18	<u>0.743±0.0002</u>	<u>13.60±0.10</u>	24.11±0.13

Table 2: **Comparison to state-of-the-art** on the *online, unconstrained* setting on NTU120-AS. → denotes that the result closer to Real is better, and ± represents 95% confidence interval. We highlight the best result in **Bold** and the second best in underline.

Method	FID↓	Acc.↑	Div.→	Multimod.→
Real	0.75±0.18	0.691±0.0093	7.15±1.27	12.94±0.96
cVAE [34]	17.33±17.14	0.552±0.0024	8.20±0.57	11.44±0.35
AGRoL [15]	64.83±277.8	<u>0.644±0.0039</u>	7.00±0.95	11.33±0.65
MDM [62]	18.40±7.95	0.647±0.0035	5.89±0.33	10.96±0.27
MDM-GRU [62]	18.63±25.87	0.574±0.0046	6.20±0.24	10.49±0.32
ReGenNet [72]	<u>13.76±4.78</u>	0.601±0.0040	6.35±0.24	<u>12.02±0.33</u>
ARFlow	10.92±3.70	0.600±0.0040	<u>6.68±0.25</u>	12.74±0.17

Table 3: **Comparison to state-of-the-art** on the *online, unconstrained* setting on Chi3D-AS. → denotes that the result closer to Real is better, and ± represents 95% confidence interval. We highlight the best result in **Bold** and the second best in underline.

4.2 Comparison to baselines

To evaluate the performance of our method, we adopt following baselines: 1) cVAE [34], commonly utilized in earlier generative models for human interactions; 2) MDM [62], the state-of-the-art diffusion-based method for human motion generation, and its variant MDM-GRU [62], which incorporates a GRU [9] backbone; 3) AGRoL [15], the current state-of-the-art method to generate full-body motions from sparse tracking signals, which adopts diffusion models with MLPs architectures; 4) ReGenNet [72], the state-of-the-art diffusion-based method for human action-reaction synthesis on online, unconstrained setting as ours. Results are taken from tables of ReGenNet [72] where all methods use 5-timestep sampling.

For the NTU120-AS dataset in Tab. 2 and Chi3D-AS dataset in Tab. 3, our proposed **ARFlow** notably outperforms baselines in terms of the FID metric, demonstrating that our method better models the mapping between the action and the reaction distribution. Our method achieves the best FID and multi-modality, second best for the action recognition accuracy and diversity on the NTU120-AS dataset and the best FID and multi-modality, second best for the diversity on the Chi3D-AS dataset. For a fair comparison, we use the pre-trained action recognition model in [72], so our action recognition accuracy is very close to the results of [72]. Given the restricted size of the Chi3D-AS test set, some fluctuations in the experimental results are to be expected. The results of InterHuman-AS dataset in Appendix B.1 show our method also yields the best results compared to baselines. As for the **offline** setting, we replace the Transformer decoder units equipped with attention masks with an 8-layer Transformer encoder architecture just like ReGenNet [72]. As demonstrated in Tab. B.2, our model also achieves superior performance on most of the metrics.

Class	Settings	FID↓	Acc.↑	Div.→	Multimod.→	Latency(ms)
	Real	0.085±0.0003	0.867±0.0002	13.063±0.0908	25.032±0.2332	-
Prediction	1) x_1	7.894±0.1814	0.743±0.0002	13.599±0.1005	24.105±0.1310	-
	2) v	14.726±0.2143	0.743±0.0002	14.154±0.0923	23.329±0.1125	-
Guidance	w. $\mathcal{L}_{\text{pene}}$	8.073±0.1981	0.741±0.0002	13.713±0.1079	24.077±0.1370	-
Timesteps	2	15.965±0.2728	0.733±0.0002	13.740±0.0896	26.767±0.1440	0.055
	5	7.894±0.1814	0.743±0.0002	13.599±0.1005	24.105±0.1310	0.111
	10	8.273±0.3862	0.721±0.0002	14.108±0.0779	22.995±0.1274	0.232
	100	8.259±0.3902	0.747±0.0002	14.173±0.1024	23.619±0.1214	2.273
Best	ARFlow	7.894±0.1814	0.743±0.0002	13.599±0.1005	24.105±0.1310	0.111

Table 4: **Ablation studies** on the *online, unconstrained* setting on the NTU120-AS dataset. **Bold** indicates the best result in our method.

4.3 Physical Constraint Guidance

Qualitative results. In Fig. 4, for the same action sequences sampled from the test sets of NTU120-AS datasets, visualization results demonstrate that both MDM and ReGenNet produce varying degrees of penetration between the actor and the reactor. In contrast, our method not only produces more physically plausible reactions, *i.e.*, mitigate penetration problems, but also more responsive reactions, *i.e.*, move backward when kicked, due to stronger modeling ability for causal relationship between actions and reactions. For more visualizations and **videos** of the generated human reactions, please refer to the supplementary materials.

Quantitative results. In Tab. 1, our ARFlow with physical constraint guidance achieves the lowest Intersection Volume, Intersection Frequency and FID than other baselines, which shows that our method achieves the lowest level of penetration while ensuring the highest generation quality. In addition, the performance is further improved through our ARFlow sampling with improved physical constraint guidance, which demonstrates the effectiveness of our guidance method. Although our guidance method effectively suppresses penetration, it also leads to a slight increase in FID, as FID only measures the similarity between generated results and the ground truth distribution and the dataset itself exists a certain degree of penetration.

4.4 Ablation Study

Network Prediction. As depicted in Tab. 3.1, a straightforward and effective strategy is to estimate clean body poses directly through a neural network, *i.e.*, \mathbf{x}_1 -prediction. We compared it with \mathbf{v} -prediction and the results are listed on the Prediction setting in Tab. 4 and Tab. B.3. Obviously, \mathbf{x}_1 -prediction has demonstrated superior performance across both settings. The reason we analyze it is that the geometric losses to regularize the generative network during the training phase directly acts on the predicted clean body poses, while \mathbf{v} -prediction requires using the predicted vector field to estimate the clean poses, so the models trained by \mathbf{x}_1 -prediction will achieve stronger overall performance.

Physical constraint guidance. As we discussed earlier, the results in Tab. 1 indicate that our physical constraint guidance can effectively suppress penetration occurrences, and it may also lead to a decrease in some other metrics shown in Tab. 4 and Tab. B.3. We also provide a qualitative comparison of the effects before and after using our physical constraint guidance in Tab. H.1. The qualitative and quantitative results demonstrated that our method achieves the lowest penetration level while maintaining the best quality of generated reactions.

Number of Euler sampling timesteps. We present comprehensive evaluation results in both online and offline scenarios, with varying Euler sampling intervals (2, 5, 10 and 100 timesteps), including the latency of reaction generation per frame on online settings and overall latency on offline settings. The experimental results, as detailed in Tab. 4 and Tab. B.3, suggest that the 5-timestep Euler sampling consistently achieves optimal performance, demonstrating superior FID scores while maintaining low latency across both evaluation settings. Thus, we adopt the 5-timestep inference as the standard configuration like [72] for all the experimental results reported in this study.

5 Conclusion

In this work, we have presented Action-Reaction Flow Matching (ARFlow), a novel framework for human action-reaction synthesis that addresses the limitations of existing diffusion-based approaches. By establishing direct action-to-reaction mappings through flow matching, ARFlow eliminates the need for complex conditional mechanisms and computationally expensive noise-to-data transformations. ARFlow involves a reprojection sampling algorithm with physical constraint guidance to enable efficient, physically plausible motion generation while preventing body penetration artifacts. Extensive evaluations on the NTU120, Chi3D and InterHuman datasets demonstrate that ARFlow excels over existing methods, showing superior performance in terms of Fréchet Inception Distance and motion diversity. Additionally, it significantly reduces body collisions, as evidenced by our new Intersection Volume and Intersection Frequency metrics.

Limitations. Although we attempt to use a reprojection method to address the issue of manifold distortions—deviations from the natural motion distribution established by flow matching, this problem still exists and our penetration loss function is just a simple design. Addressing these challenge opens a promising avenue for future theoretical research, focusing on developing guidance mechanisms that ensure physical plausibility without compromising motion authenticity.

Acknowledgement

This work was supported by National Natural Science Foundation of China (No.62406195, No.62303319), Shanghai Local College Capacity Building Program (23010503100), ShanghaiTech AI4S Initiative SHTAI4S202404, HPC Platform of ShanghaiTech University, Core Facility Platform of Computer Science and Communication of ShanghaiTech University, and MoE Key Laboratory of Intelligent Perception and Human-Machine Collaboration (ShanghaiTech University) and Shanghai Engineering Research Center of Intelligent Vision and Imaging.

References

- [1] Michael S Albergo and Eric Vanden-Eijnden. Building normalizing flows with stochastic interpolants. In *ICLR*, 2023.
- [2] Roger Alexander. Solving ordinary differential equations i: Nonstiff problems (e. hairer, sp norsett, and g. wanner). *Siam Review*, 1990.
- [3] Sadegh Aliakbarian, Pashmina Cameron, Federica Bogo, Andrew Fitzgibbon, and Thomas J Cashman. Flag: Flow-based 3d avatar generation from sparse observations. In *CVPR*, pages 13253–13262, 2022.
- [4] Tenglong Ao, Qingzhe Gao, Yuke Lou, Baoquan Chen, and Libin Liu. Rhythmic gesticulator: Rhythm-aware co-speech gesture synthesis with hierarchical neural embeddings. *TOG*, 41(6): 1–19, 2022.
- [5] Sepehr Sameni Aram Davtyan and Paolo Favaro. Efficient video prediction via sparsely conditioned flow matching. In *ICCV*, 2023.
- [6] Pablo Cervantes, Yusuke Sekikawa, Ikuro Sato, and Koichi Shinoda. Implicit neural representations for variable length human motion generation. In *ECCV*, pages 356–372. Springer, 2022.
- [7] Ricky TQ Chen, Yulia Rubanova, Jesse Bettencourt, and David K Duvenaud. Neural ordinary differential equations. *Advances in neural information processing systems*, 31, 2018.
- [8] Xin Chen, Biao Jiang, Wen Liu, Zilong Huang, Bin Fu, Tao Chen, and Gang Yu. Executing your commands via motion diffusion in latent space. In *CVPR*, 2023.
- [9] Kyunghyun Cho, Bart Van Merriënboer, Caglar Gulcehre, Dzmitry Bahdanau, Fethi Bougares, Holger Schwenk, and Yoshua Bengio. Learning phrase representations using rnn encoder-decoder for statistical machine translation. *arXiv preprint arXiv:1406.1078*, 2014.
- [10] Baptiste Chopin, Hao Tang, Naima Otberdout, Mohamed Daoudi, and Nicu Sebe. Interaction transformer for human reaction generation. *IEEE Transactions on Multimedia*, 2023.
- [11] Hyungjin Chung, Byeongsu Sim, Dohoon Ryu, and Jong Chul Ye. Improving diffusion models for inverse problems using manifold constraints. *Advances in Neural Information Processing Systems*, 35:25683–25696, 2022.
- [12] Hyungjin Chung, Jeongsol Kim, Michael T McCann, Marc L Klasky, and Jong Chul Ye. Diffusion posterior sampling for general noisy inverse problems. In *11th International Conference on Learning Representations, ICLR 2023*, 2023.
- [13] Hyungjin Chung, Jeongsol Kim, Michael Thompson Mccann, Marc Louis Klasky, and Jong Chul Ye. Diffusion posterior sampling for general noisy inverse problems. In *The Eleventh International Conference on Learning Representations*, 2023.
- [14] Rishabh Dabral, Muhammad Hamza Mughal, Vladislav Golyanik, and Christian Theobalt. Mofusion: A framework for denoising-diffusion-based motion synthesis. *arXiv preprint arXiv:2212.04495*, 2022.
- [15] Yuming Du, Robin Kips, Albert Pumarola, Sebastian Starke, Ali Thabet, and Artsiom Sanakoyeu. Avatars grow legs: Generating smooth human motion from sparse tracking inputs with diffusion model. *arXiv preprint arXiv:2304.08577*, 2023.

- [16] Patrick Esser, Sumith Kulal, Andreas Blattmann, Rahim Entezari, Jonas Müller, Harry Saini, Yam Levi, Dominik Lorenz, Axel Sauer, Frederic Boesel, et al. Scaling rectified flow transformers for high-resolution image synthesis. In *Forty-first international conference on machine learning*, 2024.
- [17] Ruiqi Feng, Tailin Wu, Chenglei Yu, Wenhao Deng, and Peiyan Hu. On the guidance of flow matching. *arXiv preprint arXiv:2502.02150*, 2025.
- [18] Mihai Fieraru, Mihai Zanfir, Elisabeta Oneata, Alin-Ionut Popa, Vlad Olaru, and Cristian Sminchisescu. Three-dimensional reconstruction of human interactions. In *CVPR*, pages 7214–7223, 2020.
- [19] Chuan Guo, Xinxin Zuo, Sen Wang, Shihao Zou, Qingyao Sun, Annan Deng, Minglun Gong, and Li Cheng. Action2motion: Conditioned generation of 3d human motions. In *ACM Multimedia*, pages 2021–2029. ACM, 2020.
- [20] Chuan Guo, Shihao Zou, Xinxin Zuo, Sen Wang, Wei Ji, Xingyu Li, and Li Cheng. Generating diverse and natural 3d human motions from text. In *Proceedings of the IEEE/CVF conference on computer vision and pattern recognition*, pages 5152–5161, 2022.
- [21] Chuan Guo, Xinxin Zuo, Sen Wang, and Li Cheng. Tm2t: Stochastic and tokenized modeling for the reciprocal generation of 3d human motions and texts. In *ECCV*, 2022.
- [22] Ikhsanul Habibie, Mohamed Elgharib, Kripasindhu Sarkar, Ahsan Abdullah, Simbarashe Nyatsanga, Michael Neff, and Christian Theobalt. A motion matching-based framework for controllable gesture synthesis from speech. In *ACM SIGGRAPH 2022 Conference Proceedings*, pages 1–9, 2022.
- [23] Gao Han, Mingjiang Liang, Jinglei Tang, Yongkang Cheng, Wei Liu, and Shaoli Huang. Reindiffuse: Crafting physically plausible motions with reinforced diffusion model. *arXiv preprint arXiv:2410.07296*, 2024.
- [24] Martin Heusel, Hubert Ramsauer, Thomas Unterthiner, Bernhard Nessler, and Sepp Hochreiter. Gans trained by a two time-scale update rule converge to a local nash equilibrium. In *NIPS*, pages 6626–6637, 2017.
- [25] Jonathan Ho and Tim Salimans. Classifier-free diffusion guidance. In *NeurIPS Workshop*, 2021.
- [26] Ludovic Hoyet, Rachel McDonnell, and Carol O’Sullivan. Push it real: Perceiving causality in virtual interactions. *ACM Transactions on Graphics (TOG)*, 31(4):1–9, 2012.
- [27] Vincent Tao Hu, Wenzhe Yin, Pingchuan Ma, Yunlu Chen, Basura Fernando, Yuki M Asano, Efstratios Gavves, Pascal Mettes, Bjorn Ommer, and Cees GM Snoek. Motion flow matching for human motion synthesis and editing. *arXiv preprint arXiv:2312.08895*, 2023.
- [28] Muhammad Gohar Javed, Chuan Guo, Li Cheng, and Xingyu Li. Intermask: 3d human interaction generation via collaborative masked modelling. *arXiv preprint arXiv:2410.10010*, 2024.
- [29] Biao Jiang, Xin Chen, Wen Liu, Jingyi Yu, Gang Yu, and Tao Chen. Motiongpt: Human motion as a foreign language. In *NeurIPS*, 2023.
- [30] Jianping Jiang, Weiye Xiao, Zhengyu Lin, Huaizhong Zhang, Tianxiang Ren, Yang Gao, Zhiqian Lin, Zhongang Cai, Lei Yang, and Ziwei Liu. Solami: Social vision-language-action modeling for immersive interaction with 3d autonomous characters. *arXiv preprint arXiv:2412.00174*, 2024.
- [31] Korrawe Karunratanakul, Konpat Preechakul, Supasorn Suwajanakorn, and Siyu Tang. Guided motion diffusion for controllable human motion synthesis. In *Proceedings of the IEEE/CVF International Conference on Computer Vision*, pages 2151–2162, 2023.
- [32] Korrawe Karunratanakul, Konpat Preechakul, Emre Aksan, Thabo Beeler, Supasorn Suwajanakorn, and Siyu Tang. Optimizing diffusion noise can serve as universal motion priors. In *Proceedings of the IEEE/CVF Conference on Computer Vision and Pattern Recognition*, pages 1334–1345, 2024.

- [33] Jihoon Kim, Jiseob Kim, and Sungjoon Choi. Flame: Free-form language-based motion synthesis & editing. *arXiv preprint arXiv:2209.00349*, 2022.
- [34] Diederik P Kingma and Max Welling. Auto-encoding variational bayes. *arXiv preprint arXiv:1312.6114*, 2013.
- [35] W. Kutta. Beitrag zur näherungsweise Integration totaler Differentialgleichungen. *Zeit. Math. Phys.*, 1901.
- [36] Matthew Le, Apoorv Vyas, Bowen Shi, Brian Karrer, Leda Sari, Rashel Moritz, Mary Williamson, Vimal Manohar, Yossi Adi, Jay Mahadeokar, et al. Voicebox: Text-guided multilingual universal speech generation at scale. In *arXiv*, 2023.
- [37] Buyu Li, Yongchi Zhao, Shi Zhelun, and Lu Sheng. Danceformer: Music conditioned 3d dance generation with parametric motion transformer. *AAAI*, 36(2):1272–1279, 2022.
- [38] Ronghui Li, Youliang Zhang, Yachao Zhang, Yuxiang Zhang, Mingyang Su, Jie Guo, Ziwei Liu, Yebin Liu, and Xiu Li. Interdance: Reactive 3d dance generation with realistic duet interactions. *arXiv preprint arXiv:2412.16982*, 2024.
- [39] Han Liang, Wenqian Zhang, Wenxuan Li, Jingyi Yu, and Lan Xu. Intergen: Diffusion-based multi-human motion generation under complex interactions. *arXiv preprint arXiv:2304.05684*, 2023.
- [40] Yaron Lipman, Ricky TQ Chen, Heli Ben-Hamu, Maximilian Nickel, and Matt Le. Flow matching for generative modeling. In *ICLR*, 2023.
- [41] Yaron Lipman, Marton Havasi, Peter Holderrieth, Neta Shaul, Matt Le, Brian Karrer, Ricky TQ Chen, David Lopez-Paz, Heli Ben-Hamu, and Itai Gat. Flow matching guide and code. *arXiv preprint arXiv:2412.06264*, 2024.
- [42] Jun Liu, Amir Shahroudy, Mauricio Perez, Gang Wang, Ling-Yu Duan, and Alex C Kot. Ntu rgb+ d 120: A large-scale benchmark for 3d human activity understanding. *T-PAMI*, 42(10): 2684–2701, 2019.
- [43] Xueyi Liu and Li Yi. Geneoh diffusion: Towards generalizable hand-object interaction denoising via denoising diffusion. *arXiv preprint arXiv:2402.14810*, 2024.
- [44] Xingchao Liu, Chengyue Gong, and Qiang Liu. Flow straight and fast: Learning to generate and transfer data with rectified flow. In *ICLR*, 2023.
- [45] Yunze Liu, Changxi Chen, and Li Yi. Interactive humanoid: Online full-body motion reaction synthesis with social affordance canonicalization and forecasting. *arXiv preprint arXiv:2312.08983*, 2023.
- [46] Yunze Liu, Changxi Chen, Chenjing Ding, and Li Yi. Physreaction: Physically plausible real-time humanoid reaction synthesis via forward dynamics guided 4d imitation. In *Proceedings of the 32nd ACM International Conference on Multimedia*, pages 3771–3780, 2024.
- [47] Ségolène Martin, Anne Gagneux, Paul Hagemann, and Gabriele Steidl. Pnp-flow: Plug-and-play image restoration with flow matching. *arXiv preprint arXiv:2410.02423*, 2024.
- [48] Kirill Neklyudov, Rob Brekelmans, Daniel Severo, and Alireza Makhzani. Action matching: Learning stochastic dynamics from samples. 2023.
- [49] Georgios Pavlakos, Vasileios Choutas, Nima Ghorbani, Timo Bolkart, Ahmed AA Osman, Dimitrios Tzionas, and Michael J Black. Expressive body capture: 3d hands, face, and body from a single image. In *CVPR*, pages 10975–10985, 2019.
- [50] Mathis Petrovich, Michael J Black, and Gül Varol. Action-conditioned 3d human motion synthesis with transformer vae. In *ICCV*, 2021.
- [51] Sigal Raab, Inbal Leibovitch, Peizhuo Li, Kfir Aberman, Olga Sorkine-Hornung, and Daniel Cohen-Or. Modi: Unconditional motion synthesis from diverse data. *arXiv preprint arXiv:2206.08010*, 2022.

- [52] Aditya Ramesh, Prafulla Dhariwal, Alex Nichol, Casey Chu, and Mark Chen. Hierarchical text-conditional image generation with clip latents. *arXiv preprint arXiv:2204.06125*, 2022.
- [53] Paul SA Reitsma and Nancy S Pollard. Perceptual metrics for character animation: sensitivity to errors in ballistic motion. In *ACM SIGGRAPH 2003 Papers*, pages 537–542. 2003.
- [54] Danilo Rezende and Shakir Mohamed. Variational inference with normalizing flows. In *International conference on machine learning*, pages 1530–1538. PMLR, 2015.
- [55] Carl Runge. Über die numerische auflösung von differentialgleichungen. *Mathematische Annalen*, 1895.
- [56] Chitwan Saharia, William Chan, Saurabh Saxena, Lala Li, Jay Whang, Emily L Denton, Kamyar Ghasemipour, Raphael Gontijo Lopes, Burcu Karagol Ayan, Tim Salimans, et al. Photorealistic text-to-image diffusion models with deep language understanding. *Advances in neural information processing systems*, 35:36479–36494, 2022.
- [57] Li Siyao, Tianpei Gu, Zhitao Yang, Zhengyu Lin, Ziwei Liu, Henghui Ding, Lei Yang, and Chen Change Loy. Duolando: Follower gpt with off-policy reinforcement learning for dance accompaniment. *arXiv preprint arXiv:2403.18811*, 2024.
- [58] Sebastian Starke, Yiwei Zhao, Taku Komura, and Kazi Zaman. Local motion phases for learning multi-contact character movements. *TOG*, 39(4):54–1, 2020.
- [59] Wenhui Tan, Boyuan Li, Chuhao Jin, Wenbing Huang, Xiting Wang, and Ruihua Song. Think then react: Towards unconstrained action-to-reaction motion generation. In *The Thirteenth International Conference on Learning Representations*.
- [60] Mikihiro Tanaka and Kent Fujiwara. Role-aware interaction generation from textual description. In *Proceedings of the IEEE/CVF International Conference on Computer Vision*, pages 15999–16009, 2023.
- [61] Jiangnan Tang, Jingya Wang, Kaiyang Ji, Lan Xu, Jingyi Yu, and Ye Shi. A unified diffusion framework for scene-aware human motion estimation from sparse signals. In *Proceedings of the IEEE/CVF Conference on Computer Vision and Pattern Recognition*, pages 21251–21262, 2024.
- [62] Guy Tevet, Sigal Raab, Brian Gordon, Yoni Shafir, Daniel Cohen-or, and Amit Haim Bermano. Human motion diffusion model. In *ICLR*, 2023.
- [63] Jie Tian, Lingxiao Yang, Ran Ji, Yuexin Ma, Lan Xu, Jingyi Yu, Ye Shi, and Jingya Wang. Gaze-guided hand-object interaction synthesis: Benchmark and method. *arXiv e-prints*, pages arXiv-2403, 2024.
- [64] Neel Trivedi, Anirudh Thatipelli, and Ravi Kiran Sarvadevabhatla. Ntu-x: an enhanced large-scale dataset for improving pose-based recognition of subtle human actions. In *Proceedings of the Twelfth Indian Conference on Computer Vision, Graphics and Image Processing*, pages 1–9, 2021.
- [65] Ashish Vaswani, Noam Shazeer, Niki Parmar, Jakob Uszkoreit, Llion Jones, Aidan N Gomez, Łukasz Kaiser, and Illia Polosukhin. Attention is all you need. *NeurIPS*, 2017.
- [66] Zhendong Wang, Jonathan J Hunt, and Mingyuan Zhou. Diffusion policies as an expressive policy class for offline reinforcement learning. In *The Eleventh International Conference on Learning Representations*, 2023.
- [67] Zhenzhi Wang, Jingbo Wang, Dahua Lin, and Bo Dai. Intercontrol: Generate human motion interactions by controlling every joint. *CoRR*, 2023.
- [68] Lemeng Wu, Dilin Wang, Chengyue Gong, Xingchao Liu, Yunyang Xiong, Rakesh Ranjan, Raghuraman Krishnamoorthi, Vikas Chandra, and Qiang Liu. Fast point cloud generation with straight flows. In *CVPR*, 2023.

- [69] Qianyang Wu, Ye Shi, Xiaoshui Huang, Jingyi Yu, Lan Xu, and Jingya Wang. Thor: Text to human-object interaction diffusion via relation intervention. *arXiv preprint arXiv:2403.11208*, 2024.
- [70] Liang Xu, Ziyang Song, Dongliang Wang, Jing Su, Zhicheng Fang, Chenjing Ding, Weihao Gan, Yichao Yan, Xin Jin, Xiaokang Yang, Wenjun Zeng, and Wei Wu. Actformer: A gan-based transformer towards general action-conditioned 3d human motion generation. *arXiv e-prints*, pages arXiv–2203, 2022.
- [71] Liang Xu, Xintao Lv, Yichao Yan, Xin Jin, Shuwen Wu, Congsheng Xu, Yifan Liu, Yizhou Zhou, Fengyun Rao, Xingdong Sheng, Yunhui Liu, Wenjun Zeng, and Xiaokang Yang. Inter-x: Towards versatile human-human interaction analysis. *arXiv preprint arXiv:2312.16051*, 2023.
- [72] Liang Xu, Yizhou Zhou, Yichao Yan, Xin Jin, Wenhan Zhu, Fengyun Rao, Xiaokang Yang, and Wenjun Zeng. Regennet: Towards human action-reaction synthesis. In *Proceedings of the IEEE/CVF Conference on Computer Vision and Pattern Recognition*, pages 1759–1769, 2024.
- [73] Sijie Yan, Yuanjun Xiong, and Dahua Lin. Spatial temporal graph convolutional networks for skeleton-based action recognition. In *AAAI*, pages 7444–7452. AAAI Press, 2018.
- [74] Sijie Yan, Zhizhong Li, Yuanjun Xiong, Huahan Yan, and Dahua Lin. Convolutional sequence generation for skeleton-based action synthesis. In *ICCV*, pages 4393–4401. IEEE, 2019.
- [75] Lingxiao Yang, Shutong Ding, Yifan Cai, Jingyi Yu, Jingya Wang, and Ye Shi. Guidance with spherical gaussian constraint for conditional diffusion. In *Proceedings of the 41st International Conference on Machine Learning*, pages 56071–56095, 2024.
- [76] Ye Yuan, Jiaming Song, Umar Iqbal, Arash Vahdat, and Jan Kautz. Physdiff: Physics-guided human motion diffusion model. In *Proceedings of the IEEE/CVF international conference on computer vision*, pages 16010–16021, 2023.
- [77] Jianrong Zhang, Yangsong Zhang, Xiaodong Cun, Shaoli Huang, Yong Zhang, Hongwei Zhao, Hongtao Lu, and Xi Shen. T2m-gpt: Generating human motion from textual descriptions with discrete representations. In *CVPR*, 2023.
- [78] Mingyuan Zhang, Zhongang Cai, Liang Pan, Fangzhou Hong, Xinying Guo, Lei Yang, and Ziwei Liu. Motiondiffuse: Text-driven human motion generation with diffusion model. *arXiv preprint arXiv:2208.15001*, 2022.
- [79] Mingyuan Zhang, Xinying Guo, Liang Pan, Zhongang Cai, Fangzhou Hong, Huirong Li, Lei Yang, and Ziwei Liu. Remodiffuse: Retrieval-augmented motion diffusion model. In *ICCV*, 2023.
- [80] Qinqing Zheng, Matt Le, Neta Shaul, Yaron Lipman, Aditya Grover, and Ricky TQ Chen. Guided flows for generative modeling and decision making. *arXiv preprint arXiv:2311.13443*, 2023.
- [81] Keyang Zhou, Bharat Lal Bhatnagar, Jan Eric Lenssen, and Gerard Pons-Moll. Toch: Spatio-temporal object-to-hand correspondence for motion refinement. In *European Conference on Computer Vision*, pages 1–19. Springer, 2022.
- [82] Yi Zhou, Connelly Barnes, Jingwan Lu, Jimei Yang, and Hao Li. On the continuity of rotation representations in neural networks. In *CVPR*, pages 5745–5753. Computer Vision Foundation / IEEE, 2019.
- [83] Zixiang Zhou and Baoyuan Wang. Ude: A unified driving engine for human motion generation. In *Proceedings of the IEEE/CVF conference on computer vision and pattern recognition*, pages 5632–5641, 2023.

ARFlow: Human Action-Reaction Flow Matching with Physical Guidance

Supplementary Materials

Appendix

A	Algorithm derivation	2
B	Experimental results on the InterHuman-AS dataset and offline settings	3
C	Influence of sampling randomness	3
D	Parameter analysis of guidance strength and weight factor	4
E	Details of our framework	4
F	Implementation details	5
G	Details of the metric calculations	5
H	User Study	6
I	Extra qualitative results	6
J	Broader Impacts	7

A Algorithm derivation

We denote the deterministic functions: $\hat{\mathbf{x}}_1 = \mathbb{E}[\mathbf{x}_1 | \mathbf{x}_t, c]$ as the \mathbf{x}_1 -prediction, $\mathbf{v}_\theta(\mathbf{x}_t, t, c) = u_t(\mathbf{x}_t)$ as the \mathbf{v} -prediction. By defining the conditional probability path as a linear interpolation between p_0 and p_1 , the intermediate process becomes:

$$\mathbf{x}_t = t\mathbf{x}_1 + [1 - (1 - \sigma_{\min})t]\mathbf{x}_0, \quad (20)$$

where $\sigma_{\min} > 0$ is a small amount of noise. Take the derivative of t on both sides:

$$\frac{d\mathbf{x}_t}{dt} = \mathbf{x}_1 - (1 - \sigma_{\min})\mathbf{x}_0, \quad (21)$$

In the marginal velocity formula, we obtain:

$$\begin{aligned} u_t(\mathbf{x}_t) &= \mathbb{E}[\mathbf{x}_1 - (1 - \sigma_{\min})\mathbf{x}_0 | \mathbf{x}_t, c] \\ &= \mathbb{E}[\mathbf{x}_1 | \mathbf{x}_t, c] - (1 - \sigma_{\min})\mathbb{E}[\mathbf{x}_0 | \mathbf{x}_t, c]. \end{aligned} \quad (22)$$

Substitute $\mathbf{x}_0 = \frac{\mathbf{x}_t - t\mathbf{x}_1}{1 - (1 - \sigma_{\min})t}$ from Eq. 20 into the above equation:

$$\begin{aligned} u_t(\mathbf{x}_t) &= \mathbb{E}[\mathbf{x}_1 | \mathbf{x}_t, c] - (1 - \sigma_{\min}) \frac{\mathbf{x}_t - t \mathbb{E}[\mathbf{x}_1 | \mathbf{x}_t, c]}{1 - (1 - \sigma_{\min})t} \\ &= \frac{\mathbb{E}[\mathbf{x}_1 | \mathbf{x}_t, c] - (1 - \sigma_{\min})\mathbf{x}_t}{1 - (1 - \sigma_{\min})t} \end{aligned}$$

where we have used the fact that $E[\mathbf{x}_t | \mathbf{x}_t] = \mathbf{x}_t$. According to $\hat{\mathbf{x}}_1 = \mathbb{E}[\mathbf{x}_1 | \mathbf{x}_t, c]$, $\mathbf{v}_\theta(\mathbf{x}_t, t, c) = u_t(\mathbf{x}_t)$, we get the equivalent form of parameterization:

$$\mathbf{v}_\theta(\mathbf{x}_t, t, c) = \frac{\hat{\mathbf{x}}_1 - (1 - \sigma_{\min})\mathbf{x}_t}{1 - (1 - \sigma_{\min})t}, \quad (23)$$

Substitute Eq. 23 into the following equation:

$$\begin{aligned} \mathbf{x}_{t'} &= \mathbf{x}_t - (t - t')\mathbf{v}_\theta(\mathbf{x}_t, t, c) \\ &= \mathbf{x}_t - (t - t') \frac{\hat{\mathbf{x}}_1 - (1 - \sigma_{\min})\mathbf{x}_t}{1 - (1 - \sigma_{\min})t} \\ &= \frac{1 - (1 - \sigma_{\min})t'}{1 - (1 - \sigma_{\min})t} \mathbf{x}_t + \frac{t' - t}{1 - (1 - \sigma_{\min})t} \hat{\mathbf{x}}_1. \end{aligned} \quad (24)$$

Finally, let $t = t_n$ and $t' = t_{n+1}$, we can obtain the estimation of $\hat{\mathbf{x}}_1$ from Eq. 23:

$$\hat{\mathbf{x}}_1 \leftarrow (1 - \sigma_{\min})\mathbf{x}_{t_n} + (1 - (1 - \sigma_{\min})t_n) \mathbf{v}_\theta(\mathbf{x}_{t_n}, t_n, \mathbf{c}), \quad (25)$$

and our sampling formulation based on \mathbf{x}_1 -prediction from Eq. 24:

$$\mathbf{x}'_{t_{n+1}} \leftarrow \frac{1 - (1 - \sigma_{\min})t_{n+1}}{1 - (1 - \sigma_{\min})t_n} \mathbf{x}_{t_n} + \frac{t_{n+1} - t_n}{1 - (1 - \sigma_{\min})t_n} \hat{\mathbf{x}}_1. \quad (26)$$

Algorithm 3 Sampling algorithm with vanilla guidance of physical constraints. (\mathbf{v} -prediction)

- 1: **Input:** $\mathcal{L}_{\text{pene}}$ the loss function ; \mathbf{v} and θ the vector field predictor with pretrained parameters
 - 2: **Parameters:** N the number of sampling steps; λ_{pene} the scale factor to control the strength of guidance
 - 3: Sample \mathbf{x}_0 from the action distribution
 - 4: **for** $n = 1, 2, \dots, N - 1$ **do**
 - 5: # Estimate $\hat{\mathbf{x}}_1$ (Eq. 25)
 - 6: $\hat{\mathbf{x}}_1 \leftarrow (1 - \sigma_{\min})\mathbf{x}_{t_n} + (1 - (1 - \sigma_{\min})t_n) \mathbf{v}_\theta(\mathbf{x}_{t_n}, t_n, \mathbf{c})$
 - 7: # Flow matching \mathbf{v} -prediction sampling (Eq. 8)
 - 8: $\mathbf{x}'_{t_{n+1}} \leftarrow \mathbf{x}_{t_n} + (t_{n+1} - t_n) \mathbf{v}_\theta(\mathbf{x}_{t_n}, t_n, \mathbf{c})$
 - 9: # Physical constraint guidance
 - 10: $\mathbf{x}_{t_{n+1}} \leftarrow \mathbf{x}'_{t_{n+1}} + \lambda_{\text{pene}} \nabla_{\mathbf{x}_{t_n}} \mathcal{L}_{\text{pene}}(\hat{\mathbf{x}}_1)$
 - 11: **end for**
 - 12: **Return:** The reaction motion after guidance $\mathbf{x}_1 = \mathbf{x}_{t_N}$
-

Methods	R Precision (Top 3) \uparrow	FID \downarrow	MM Dist \downarrow	Diversity \rightarrow	MModality \uparrow
Real	0.722 \pm 0.004	0.002 \pm 0.0002	3.503 \pm 0.011	5.390 \pm 0.058	-
T2M [20]	0.224 \pm 0.003	32.482 \pm 0.0975	7.299 \pm 0.016	4.350 \pm 0.073	0.719 \pm 0.041
MDM [62]	0.370 \pm 0.006	3.397 \pm 0.0352	8.640 \pm 0.065	4.780 \pm 0.117	2.288 \pm 0.039
MDM-GRU [62]	0.328 \pm 0.012	6.397 \pm 0.2140	8.884 \pm 0.040	4.851 \pm 0.081	2.076 \pm 0.040
RAIG [60]	0.363 \pm 0.008	2.915 \pm 0.0292	7.294 \pm 0.027	4.736 \pm 0.099	2.203 \pm 0.049
InterGen [39]	0.374 \pm 0.005	13.237 \pm 0.0352	10.929 \pm 0.026	4.376 \pm 0.042	2.793\pm0.014
ReGenNet [72]	0.407 \pm 0.003	2.265 \pm 0.0969	6.860 \pm 0.0040	5.214 \pm 0.139	2.391 \pm 0.023
ARFlow	0.434\pm0.003	1.637\pm0.0413	3.949\pm0.0042	5.259\pm0.117	2.502 \pm 0.021

Table B.1: **Comparison to state-of-the-arts** on the *online, unconstrained* setting for human action-reaction synthesis on the InterHuman-AS dataset. \rightarrow denotes that the result closer to Real is better, and \pm represents 95% confidence interval. We highlight the best result in **Bold**.

Method	FID \downarrow	Acc. \uparrow	Div. \rightarrow	Multimod. \rightarrow
Real	0.09 \pm 0.00	0.867 \pm 0.0002	13.06 \pm 0.09	25.03 \pm 0.23
cVAE [34]	74.73 \pm 4.86	0.760 \pm 0.0002	11.14 \pm 0.04	18.40 \pm 0.26
AGRoL [15]	16.55 \pm 1.41	0.716 \pm 0.0002	13.84 \pm 0.10	21.73 \pm 0.20
MDM [62]	7.49 \pm 0.62	0.775\pm0.0003	<u>13.67\pm0.18</u>	24.14 \pm 0.29
MDM-GRU [62]	24.25 \pm 1.39	0.720 \pm 0.0002	13.43\pm0.09	22.24 \pm 0.29
ReGenNet [72]	<u>6.19\pm0.33</u>	0.772 \pm 0.0003	14.03 \pm 0.09	<u>25.21\pm0.34</u>
ARFlow	5.00\pm0.17	<u>0.772\pm0.0002</u>	13.84 \pm 0.09	25.10\pm0.17

Table B.2: **Results** on the *offline, unconstrained* setting on NTU120-AS. We highlight the best result in **Bold** and the second best in underline.

B Experimental results on the InterHuman-AS dataset and offline settings

For the text-conditioned setting, we adopt T2M [20], MDM [62], MDM-GRU [62], RAIG [60] and InterGen [39] as baselines. Tab. B.1 shows our method also yields the best results compared to baselines. To demonstrate the universality of our ARFlow and physical guidance methods, we also conducted offline setting experiments in Tab.B.2 and Tab.B.3.

C Influence of sampling randomness

As depicted in Tab. C.1, although stochastic sampling increases the diversity of generated reaction motions, it sometimes has some impact on the quality of the sample due to its stochastic nature.

Class	Settings	FID \downarrow	Acc. \uparrow	Div. \rightarrow	Multimod. \rightarrow	Latency(ms)
	Real	0.085 \pm 0.0003	0.867 \pm 0.0002	13.063 \pm 0.0908	25.032 \pm 0.2332	-
Prediction	1) x_1	5.003\pm0.1654	0.762\pm0.0002	13.844 \pm 0.0905	25.104\pm0.1704	-
	2) v	7.585 \pm 0.1562	0.757 \pm 0.0002	13.775 \pm 0.0982	24.200 \pm 0.1355	-
Guidance	w. $\mathcal{L}_{\text{pene}}$	5.048 \pm 0.1167	0.750 \pm 0.0002	13.838 \pm 0.0893	25.048 \pm 0.1595	-
Timesteps	2	7.936 \pm 0.1581	0.759 \pm 0.0002	14.538 \pm 0.1016	25.904 \pm 0.1754	0.023
	5	5.003\pm0.1654	0.762\pm0.0002	13.844 \pm 0.0905	25.104\pm0.1704	0.053
	10	5.506 \pm 0.1657	0.744 \pm 0.0002	13.870 \pm 0.0942	24.732 \pm 0.1533	0.110
	100	5.836 \pm 0.3763	0.748 \pm 0.0002	13.635 \pm 0.0948	24.058 \pm 0.1371	1.132
Best	ARFlow	5.003\pm0.1654	0.762\pm0.0002	13.844 \pm 0.0905	25.104\pm0.1704	0.053

Table B.3: **Ablation studies** on the *offline, unconstrained* setting on the NTU120-AS dataset. **Bold** indicates the best result in our method.

Method	Settings	FID↓	Acc.↑	Div.→	Multimod.→
	Real	0.085±0.0003	0.867±0.0002	13.063±0.0908	25.032±0.2332
Randomness β	0.05	13.821±0.2895	0.709±0.0003	14.002±0.1055	24.269±0.1363
	0.02	8.060±0.1517	0.728±0.0002	13.928±0.1076	24.161±0.1512
	0.01	7.671±0.1357	0.728±0.0002	13.895±0.1080	24.114±0.1486
ARFlow	0	7.894±0.1814	0.743±0.0002	13.599±0.1005	24.105±0.1310

Table C.1: **Randomness Influence studies** on the *online, unconstrained* setting on the NTU120-AS dataset. **Bold** indicates the best result in our method.

D Parameter analysis of guidance strength and weight factor

We conduct a parameter analysis of guidance strength in Tab. D.1. The result of the experiments show that as the guiding strength increases, the degree of penetration between actors and reactors decreases significantly, while FID increases slightly. This is because the ground truth itself has a certain degree of penetration. Thus, this task requires our new metrics and FID to collaborate in evaluating the quality of the generated results. When the guidance strength increases to a certain extent, the decrease in penetration degree is no longer significant. Therefore, we ultimately choose $\lambda_{\text{pene}} = 2$. Our method achieves the lowest penetration level while maintaining the best generation quality. As for the weight factor, the results show that the minimum value of FID does not occur at the endpoints, thus demonstrating the effectiveness of our weighting method.

Table D.1: Parameter analysis of guidance strength and weight factor on the *online, unconstrained* setting on NTU120-AS. **Bold** indicates the best result.

Parameter	settings	FID ↓	IF ↓	IV ↓
	Real	0.09	21.96%	5.35
λ_{pene}	0	7.89	8.39%	3.26
	1	7.98	5.80%	1.15
	2	8.20	3.54%	0.68
	5	8.49	1.22%	0.13
	10	9.41	0.78%	0.21
w	0	8.37	2.71%	0.35
	0.1	8.30	2.78%	0.36
	0.3	8.19	2.96%	0.37
	0.5	8.11	3.12%	0.41
	0.7	8.07	3.23%	0.53
	0.9	8.08	3.32%	0.64
	1	8.20	3.54%	0.68

E Details of our framework

We present our Human Action-Reaction Flow Matching (ARFlow) framework, illustrated in Fig. 2, which comprises a flow module and a Transformer decoder G . Given a paired action-reaction sequence and an optional signal c (e.g., an action label, dotted lines in Fig. 2), $\langle x_0^{1:H}, x_1^{1:H}, c \rangle$, $x_1^{1:H}$ represents the reaction to generate. For a sampled timestep t , we linearly interpolate $x_1^{1:H}$ and $x_0^{1:H}$ as Eq. 4 to produce the $x_t^{1:H}$. Then the $x_t^{1:H}$ turns into the latent features through an FC layer to dimension d . The timestep t and the optional condition c are separately projected to dimension d using feed-forward networks and combined to form the token z . The Transformer decoder G , implemented with stacked 8 layers, prevents future information leakage through masked multi-head attention, enabling *online* generation as in [72]. Decoder G takes z as input tokens and $x_t^{1:H}$ combined with a standard positional embedding as output tokens, along with a directional attention mask to ensure the model cannot access future actions at the current timestep. The decoder’s output is projected back to produce the predicted clean body poses $\hat{x}_1^{1:H}$. Online reaction generation is achieved in an auto-regressive manner, following the approach of [72]. The intention branch can

be activated when the actor’s intention is accessible to the reactor, or deactivated otherwise. The directional attention mask can be turned off for offline settings.

At the inference stage, we employ our physical constraint guidance method. After training latent linear layers and Transformer decoder G , our ARFlow uses them for x_1 -prediction based sampling. The sampling process is further guided by the gradient of \mathcal{L}_{pene} to generate physically plausible reactions.

F Implementation details

Our ARFlow model is trained with $T = 1,000$ timesteps using a classifier-free approach [25]. The number of decoder layers is 8 and the latent dimension of the Transformer tokens is 512. The batch size is configured as 32 for NTU120-AS, InterHuman-AS and 16 for Chi3D-AS. The interaction loss weight is set to $\lambda_{inter} = 1$. Each model is trained for 500K steps on single NVIDIA 4090 GPU within 48 hours. During inference, unless otherwise stated, we employ 5-timestep sampling for all the diffusion-based and our models in our experiments as [72] for a fair comparison. For the physical constraint guidance, we set the safe distance $\zeta = 0.5$, $\lambda_{pene} = 2$ and $w = 0.7$.

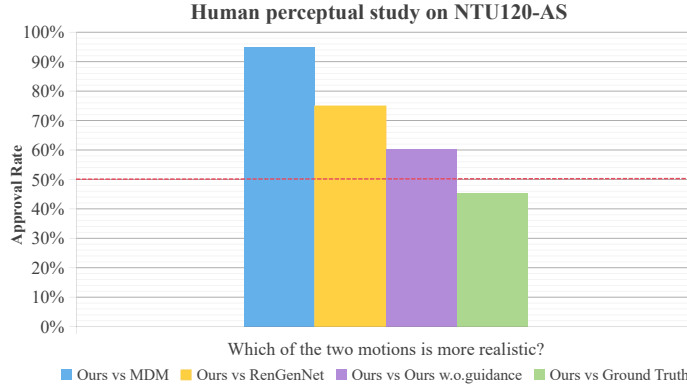


Figure F.1: Human perceptual study results on NTU120-AS.

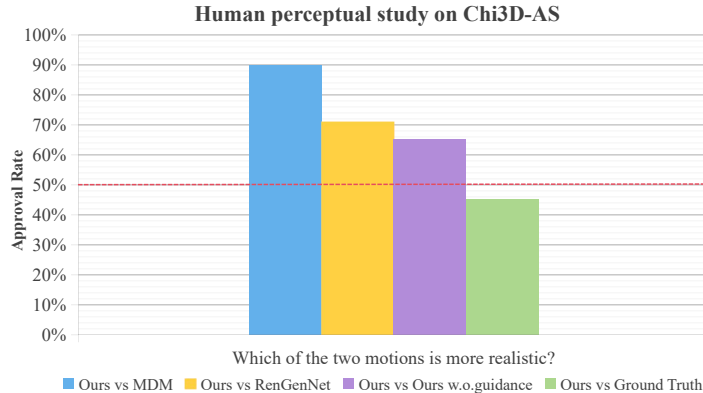


Figure F.2: Human perceptual study results on Chi3D-AS.

G Details of the metric calculations

We follow the prior works in human action-reaction synthesis, ReGenNet [72] and MDM [62] to calculate the Frechet Inception Distance(FID) [24], action recognition accuracy, diversity and multi-modality. For a fair comparison, we use the pre-trained action recognition model in [72], which is a slightly modified version of ST-GCN [73]. The model takes the 6D rotation representation of the SMPL-X parameters as input and outputs classification results of action-reaction pairs. We generate 1,000 reaction samples by sampling actor motions from test sets and evaluate each method 20 times using different random seeds to calculate the average with the 95% confidence interval.

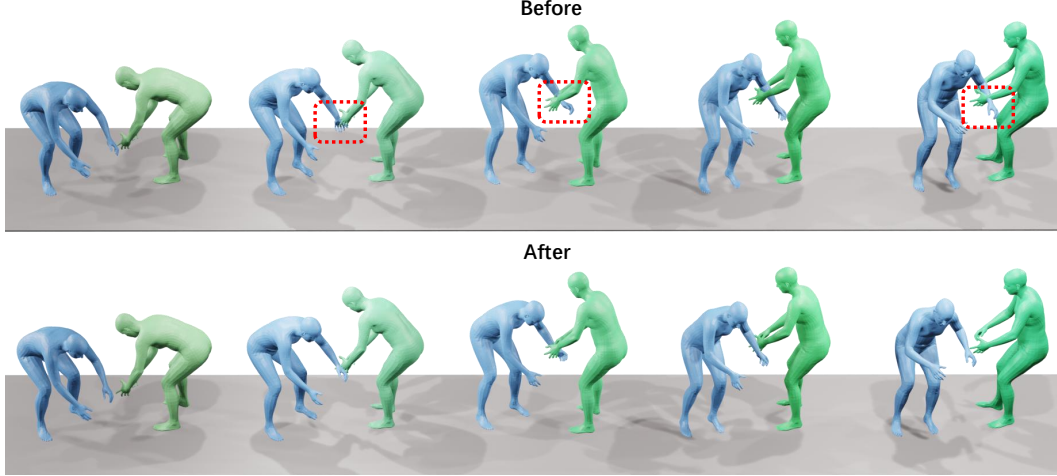


Figure H.1: **Visualization comparison** of the effects before and after using physical constraint guidance. **Blue** for actors and **Green** for reactors.

1) Frechet Inception Distance (FID) [24] measures the similarity in feature space between predicted and ground-truth motion; 2) Action Recognition Accuracy (Acc.) assesses how likely a generated motion can be successfully recognized. We adopt the pre-trained ST-GCN model to classify the generated results; 3) Diversity (Div.) evaluates feature diversity within generated motions. Given the motion feature vectors of generated motions and real motions as $\{v_1, \dots, v_{S_d}\}$ and $\{v'_1, \dots, v'_{S_d}\}$, the diversity is defined as $Diversity = \frac{1}{S_d} \sum_{i=1}^{S_d} \|v_i - v'_i\|_2$. $S_d = 200$ in our experiments. 4) Multimodality (Multimod.) quantifies the ability to generate multiple different motions for the same action type. Given a collection of motions containing C action types, for c -th action, we randomly sample two subsets of size S_l , and then extract the corresponding feature vectors as $\{v_{c,1}, \dots, v_{c,S_l}\}$ and $\{v'_{c,1}, \dots, v'_{c,S_l}\}$, the multimodality is defined as $Multimod. = \frac{1}{C \times S_l} \sum_{c=1}^C \sum_{i=1}^{S_l} \|v_{c,i} - v'_{c,i}\|_2$. $S_l = 20$ in our experiments. 5) Intersection Volume (IV) measures the volume of human-human inter-penetration by voxelizing actor and reactor meshes and reporting the volume of voxels occupied by both. 6) Intersection Frequency (IF) measures the frequency of inter-penetration. We generate 260 samples for evaluation.

H User Study

We conducted a human perceptual study to investigate the quality of the motions generated by our model. We invite 20 users to provide four comparisons. For each comparison, we ask the users “Which of the two motions is more realistic?”, and each user is provided 10 sequences to evaluate.

The results are shown in Fig. F.1 and Fig. F.2. Our results were preferred over the other state-of-the-art and are even competitive with ground truth motions.

I Extra qualitative results

We show the generated motions of our method against others in Fig. I.1. We highlight the implausible motions in rectangle marks, it is clear that our method learns the correct reactions and avoids human-human inter-penetrations as much as possible.

Failure case. We also show the failure cases of our motion generation pipeline in Fig. I.2. Our model cannot guarantee absolute physical authenticity, for example, ensuring that the hand contacts but does not penetrate during handshaking. Incorporating more sophisticated physical constraints may solve the failure cases and be considered in future.

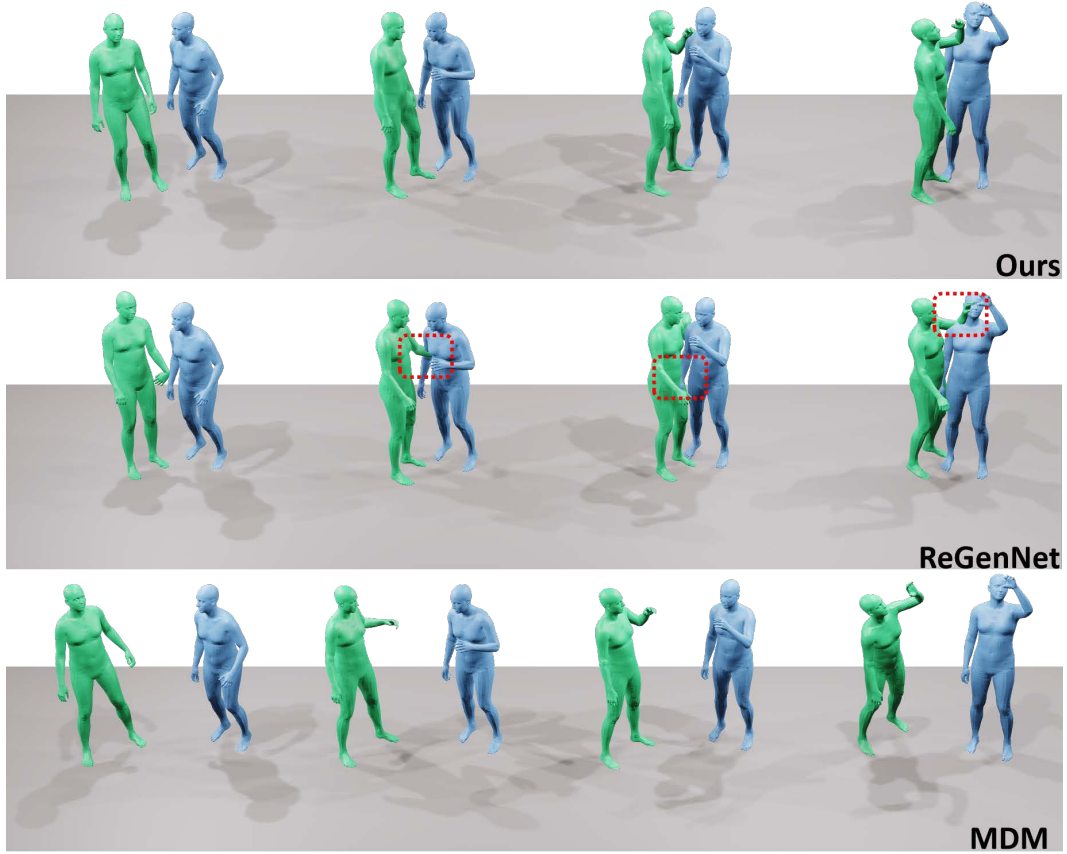


Figure I.1: The extra qualitative experiment. **Blue** for actors and **Green** for reactors.

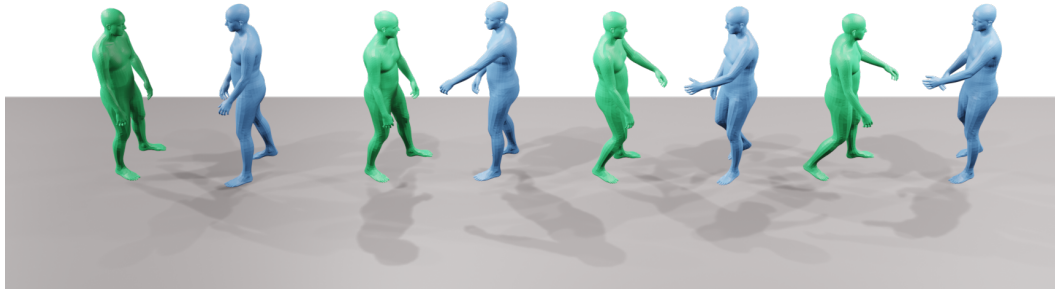


Figure I.2: Failure case of our method.

J Broader Impacts

Our model demonstrates significant potential for AR/VR and gaming applications by enabling the generation of plausible human reactions. Beyond virtual environments, the proposed approach provides an innovative technical pathway for real-world human-robot interaction, where motion patterns can be transferred to robotic systems through motion remapping technology. Although this advancement may inspire future research, we acknowledge potential misuse risks similar to other generative models, warranting ethical considerations as the technology develops.